New Journal of Physics
The open access journal at the forefront of physics
Deutsche Physikalische Gesellschaft DPG IOP Institute of Physics

PAPER • OPEN ACCESS

Broadband tunable transmission non-reciprocity in thermal atoms dominated by two-photon transitions

To cite this article: Hui-Min Zhao *et al* 2024 *New J. Phys.* **26** 043018

IOP Publishing New J. Phys. 26 (2024) 043018 https://doi.org/10.1088/1367-2630/ad3d7a

New Journal of Physics
The open access journal at the forefront of physics

Deutsche Physikalische Gesellschaft DPG
IOP Institute of Physics
Published in partnership with: Deutsche Physikalische Gesellschaft and the Institute of Physics

OPEN ACCESS

RECEIVED
19 February 2024

REVISED
22 March 2024

ACCEPTED FOR PUBLICATION
11 April 2024

PUBLISHED
23 April 2024

PAPER

Broadband tunable transmission non-reciprocity in thermal atoms dominated by two-photon transitions

Hui-Min Zhao[1], **Di-Di Zheng**[2], **Xiao-Jun Zhang**[1,*] and **Jin-Hui Wu**[1,*]

[1] Center for Quantum Sciences and School of Physics, Northeast Normal University, Changchun 130024, People's Republic of China
[2] School of Mechanics and Optoelectronic Physics, Anhui University of Science and Technology, Huainan 232001, People's Republic of China
[*] Authors to whom any correspondence should be addressed.

E-mail: zhangxj037@nenu.edu.cn and jhwu@nenu.edu.cn

Keywords: broadband and tunable optical non-reciprocity, single-photon far-detuned transition, two-photon near-resonant transition, Doppler broadening reduction, frequency and amplitude modulation, intersecting angle control

Abstract

We propose a scheme for realizing broadband and tunable transmission non-reciprocity by utilizing two-photon near-resonant transitions in thermal atoms as single-photon far-detuned transitions can be eliminated. Our basic idea is to largely reduce the Doppler broadenings on a pair of two-photon, probe and coupling, transitions and meanwhile make the only four-photon transition Doppler-free (velocity-dependent) for a forward (backward) probe field. One main advantage of this scheme lies in that the transmission non-reciprocity can be realized and manipulated in a frequency range typically exceeding 200 MHz with isolation ratio above 20 dB and insertion loss below 1.0 dB by modulating an assistant field in frequency and amplitude. The intersecting angle between four applied fields also serves as an effective control knob to optimize the nonreciprocal transmission of a forward or backward probe field, e.g. in a much wider frequency range approaching 1.4 GHz.

1. Introduction

Nonreciprocal optical devices [1–4] permitting photon transport in one direction but not in the opposite direction, like isolators and circulators, are essential in a wide range of modern science and technology, ranging from classical light communications to quantum information processing. Though a lot of advances have been made, it is still challenging to achieve optical non-reciprocity with high isolation ratios and low insertion losses for weak light signals due to the time-reversal symmetry of most (linear) optical materials. Traditionally, magneto-optical media are used to break the time-reversal symmetry with the Faraday rotation effect, which requires however bulky magnets making against real applications involving integrated photonic devices [5–8]. Hence, significant efforts have been made recently to develop the magnet-free optical non-reciprocity by exploring different mechanisms, including nonlinear effects [9–17], spatiotemporal modulations [18–22], optomechanical interactions [23–28], moving atomic lattices [29–31], chiral quantum systems [32–36], and atomic thermal motions [37–46]. Note also that nonreciprocal amplification has aroused particular interests and achieved significant progresses since it can facilitate the optical read-out of sensitive signals and simplify the construction of complex optical networks by avoiding the amplification of undesired reflections [46–48].

Magnet-free optical isolation exploiting thermal atoms coherently driven into the regime of electromagnetically induced transparency (EIT) is conceptually different and admirable because relevant realizations are simpler than those utilizing other mechanisms. In the typical three-level Λ configuration, for instance, the EIT response of thermal atoms may exhibit a broken time-reversal symmetry with the underlying quantum destructive interference depending critically on the propagation directions of a weak probe and a strong coupling field [37–39, 46]. That is, a forward (backward) probe field will experience a high (low) transmissivity due to the well preserved (largely destroyed) quantum destructive interference when its two-photon resonance along with a forward coupling field is kept Doppler-free (velocity-dependent), which can be operated even at the single-photon level [45]. Such an interesting mechanism utilizing the direction-dependent interplay of EIT responses and Doppler broadenings has been extended to the four-level N configuration, exhibiting a chiral cross-Kerr nonlinear response for a probe field coming from two opposite directions [2, 40, 41, 46].

Previous studies are limited to only single-photon transitions, which can be made under appropriate conditions however negligible as compared to two-photon transitions by eliminating some intermediate states [49]. This motivates us to consider whether the direction-dependent EIT mechanism for achieving a transmission non-reciprocity, if extended to two-photon transitions [50], will provide some advantages and additional degrees of manipulation? In fact, most previous studies examine the non-reciprocal transmission of a single probe field due to limited natural linewidths of single-photon transitions, though it is possible to achieve the nonreciprocal bandwidths over 100 MHz and up to 1.0 GHz through nonlinear optical processes [41–43]. It is also known that the simultaneous manipulation of a vast number of light signals is required in all-optical networks, and wavelength division multiplexing (WDM) [51–53] is an effective technique for enlarging the information capacity of optical fiber communication [54–59]. Then, a specific question arises, whether the linear non-reciprocal transmission, if extended to systems dominated by two-photon transitions, can be realized in a wide enough frequency range appropriate for the WDM manipulation of multiple probe fields?

With above considerations, here we investigate a five-level Λ system for achieving two-photon EIT responses sensitive to the propagating direction of a probe field as it can be reduced to a three-level Λ system with two intermediate states being adiabatically eliminated. This is attained by making a probe and an assistant field as well as two coupling fields to keep two-photon near resonance, respectively, when the two pairs of oppositely propagating fields are far detuned from relevant single-photon transitions. Taking thermal atoms into account, we find that the probe field incident upon one side exhibits very low losses while that upon the other side is strongly absorbed in a frequency range of tens of natural linewidths (>200 MHz) controlled by the assistant field. This broadband transmission non-reciprocity, facilitating WDM, of high isolation ratios (> 20 dB) and low insertion losses (<1.0 dB) is a result of the direction-dependent Doppler effect on the only four-photon transition and the largely reduced Doppler broadenings on both two-photon transitions. It is also of interest that the intersecting angle between the two pairs of oppositely traveling fields can be tuned to realize a broader nonreciprocal bandwidth (i.e. up to 1.4 GHz for instance).

2. Model & equations

We consider in figure 1(a) a five-level atomic system coherently driven into the Λ configuration with two lower ground states $|1\rangle$ and $|2\rangle$, two intermediate excited states $|3\rangle$ and $|4\rangle$, and an upper excited state $|5\rangle$. A probe field of frequency ω_p (amplitude E_p), an assistant field of frequency ω_a (amplitude E_a), a first coupling field of frequency ω_{c1} (amplitude E_{c1}) and a second coupling field of frequency ω_{c2} (amplitude E_{c2}) act upon four transitions $|1\rangle \leftrightarrow |3\rangle$, $|3\rangle \leftrightarrow |5\rangle$, $|2\rangle \leftrightarrow |4\rangle$, and $|4\rangle \leftrightarrow |5\rangle$, respectively. The corresponding (real) Rabi frequencies are $\Omega_p = d_{13}E_p/2\hbar$, $\Omega_a = d_{35}E_a/2\hbar$, $\Omega_{c1} = d_{24}E_{c1}/2\hbar$, and $\Omega_{c2} = d_{45}E_{c2}/2\hbar$, respectively, with d_{mn} being electric dipole moment on transition $|m\rangle \leftrightarrow |n\rangle$. In addition, we have defined $\Delta_p = \omega_p - \omega_{31}$ and $\Delta_a = \omega_a - \omega_{53}$ as single-photon detunings on the two left-arm transitions while $\Delta_{c1} = \omega_{c1} - \omega_{42}$ and $\Delta_{c2} = \omega_{c2} - \omega_{54}$ as single-photon detunings on the two right-arm transitions. To be more specific, here we consider ^{87}Rb atoms as an example with hyperfine states $|1\rangle = |5S_{1/2}, F=1\rangle$, $|2\rangle = |5S_{1/2}, F=2\rangle$, $|3\rangle = |5P_{1/2}, F=1\rangle$, $|4\rangle = |5P_{1/2}, F=2\rangle$, and $|5\rangle = |7S_{1/2}, F=2\rangle$, exhibiting transition wavelengths $\lambda_p = \lambda_{c1} = 795.0$ nm and $\lambda_a = \lambda_{c2} = 728.7$ nm as well as spontaneous decay rates $\Gamma_{31} = \Gamma_{32} = \Gamma_{41} = \Gamma_{42} = 2.87$ MHz and $\Gamma_{53} = \Gamma_{54} = 0.19$ MHz [60, 61]. Zeeman sublevels are not specified since all of them will be inevitably populated due to random atomic collisions.

Then, under the electric-dipole and rotating-wave approximations, it is straightforward to construct the interaction Hamiltonian H_I and write down dynamic equations for the five-level Λ system with respect to 25 density matrix elements ρ_{mn} for $\{m,n\} \in \{1,2,3,4,5\}$ [62]. Setting $\Delta_p + \Delta_a \simeq 0$ and $\Delta_{c1} + \Delta_{c2} \simeq 0$ to enable near-resonant two-photon transitions while $|\Delta_{p,a}| \gg \Omega_{p,a}$ and $|\Delta_{c1,c2}| \gg \Omega_{c1,c2}$ to ensure large single-photon detunings, it is viable to simplify the five-level Λ system into a three-level Λ system as shown in figure 1(b) described by an effective Hamiltonian H_e. The validity for eliminating intermediate states $|3\rangle$ and $|4\rangle$ can be verified by comparing probe absorption spectra obtained by solving density matrix equations for the five-level Λ system and those for the three-level Λ system. Details for above discussions are given in the two appendices, where we have introduced Rabi frequency $\Omega_{pe} = -\Omega_p\Omega_a/\Delta_p$ ($\Omega_{ce} = -\Omega_{c1}\Omega_{c2}/\Delta_{c2}$) for the effective probe (coupling) field and dynamic Stark shift $\Delta_{2d} \simeq -|\Omega_{c1}|^2/\Delta_{c1}$ ($\Delta_{5d} \simeq |\Omega_a|^2/\Delta_a + |\Omega_{c2}|^2/\Delta_{c2}$) for the ground (upmost) state $|2\rangle$ ($|5\rangle$).

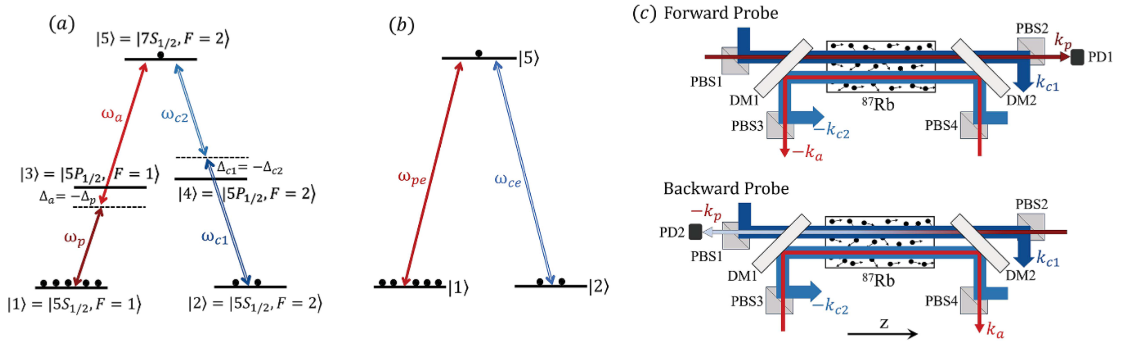

Figure 1. (a) An original five-level Λ system driven by a probe field ω_p, an assistant field ω_a, and two coupling fields $\omega_{c1,c2}$ set with large single-photon detunings while in appropriate two-photon resonances. Energy levels $|1\rangle$, $|2\rangle$, $|3\rangle$, $|4\rangle$, and $|5\rangle$ refer, respectively, to hyperfine states $|5S_{1/2}, F=1\rangle$, $|5S_{1/2}, F=2\rangle$, $|5P_{1/2}, F=1\rangle$, $|5P_{1/2}, F=2\rangle$, and $|5\rangle = |7S_{1/2}, F=2\rangle$ of ^{87}Rb atoms. (b) An equivalent three-level Λ system driven by an effective probe field $\omega_{pe} = \omega_p + \omega_a$ and an effective coupling field $\omega_{ce} = \omega_{c1} + \omega_{c2}$ on different two-photon transitions. (c) An illustration of nonreciprocal light propagation in warm ^{87}Rb atoms for counter-traveling probe fields with wavevectors k_p and $-k_p$, respectively. Other fields have been arranged to largely reduce Doppler broadenings on both two-photon transitions with effective probe $\pm k_{pe} = \pm(k_p - k_a)$ and coupling $k_{ce} = k_{c1} - k_{c2}$ wavevectors. PBS1-PBS4: polarization beam splitters; DM1-DM2: dichroic mirrors; PD1-PD2: photodetectors.

In the limit of a weak effective probe field ($\Omega_{pe} \to 0$), solving the three-level Λ system by setting $\partial_t \rho_{mn} = 0$, we can obtain the atomic population in state $|5\rangle$

$$\rho_{55} = \frac{2\gamma |\Omega_{pe}|^2 \Delta_{12e}^2 / \Gamma}{|\Omega_{ce}|^4 - 2|\Omega_{ce}|^2 \Delta_{12e}\Delta_{15e} + (\Gamma^2 + \Delta_{15e}^2)\,\Delta_{12e}^2}, \tag{1}$$

with $\Delta_{12e} = \Delta_{12} + \Delta_{2d}$ and $\Delta_{15e} = \Delta_{15} + \Delta_{5d}$ being effective detunings on transitions $|1\rangle \leftrightarrow |2\rangle$ and $|1\rangle \leftrightarrow |5\rangle$, respectively. We have considered $\Gamma_{51} = \Gamma_{52} = \Gamma$ for the chosen states of ^{87}Rb atoms and $\gamma_{51} = \gamma_{52} = \Gamma + \gamma_l$ with γ_l being the common linewidth of all laser fields while neglecting the much smaller decoherence rate γ_{21} arising from atomic collisions. Then it is viable to further obtain the absorption coefficient and the probe transmissivity (see the appendix B) as given below

$$\alpha_p = \frac{N d_{13}^2}{\hbar \varepsilon_0} \frac{\pi \Gamma}{\lambda_p} \frac{\rho_{55}}{|\Omega_p|^2}, \tag{2a}$$

$$T_p = e^{-\alpha_p L}, \tag{2b}$$

where N and L are introduced to denote the density and length of a thermal atomic sample, respectively.

With thermal atoms under consideration, frequencies of the probe, assistant, and two coupling fields are shifted to different extents for different atoms of velocity v in a Maxwell distribution depending on their propagating directions. In this regard, we have a total of sixteen geometric arrangements for the Doppler shifts of four applied fields as they propagate along either the z or the $-z$ direction. Two among these arrangements, referred to as the cases of *(i) forward* and *(ii) backward* probes, are of our special interest as shown in figure 1(c). In both cases, the probe and assistant fields of horizontal linear polarization as well as the two coupling fields of vertical linear polarization have been arranged to propagate in the opposite directions so as to well suppress the Doppler broadenings on two-photon transitions $|1\rangle \leftrightarrow |5\rangle$ and $|2\rangle \leftrightarrow |5\rangle$. This is realized by separating light beams of horizontal and vertical polarizations via four polarization beam splitters PBS1-PBS4 while light beams of wavelengths 795.0 nm and 728.7 nm via two dichroic mirrors DM1-DM2.

More specifically, the single-photon detunings should be replaced by $\Delta_p + k_p v$, $\Delta_a - k_a v$, $\Delta_{c1} + k_{c1} v$, and $\Delta_{c2} - k_{c2} v$ in case (i) while by $\Delta_p - k_p v$, $\Delta_a + k_a v$, $\Delta_{c1} + k_{c1} v$, and $\Delta_{c2} - k_{c2} v$ in case (ii) with '+' and '−' denoting the z and $-z$ directions, respectively. Here we have introduced wavenumbers $k_i = 2\pi/\lambda_i$ and wavelengths λ_i for relevant light fields with $i \in \{p, a, c1, c2\}$. Accordingly, the two-photon detunings should be replaced by $\Delta_{15} + k_{pe} v$ and $\Delta_{15} - \Delta_{12} + k_{ce} v$ in case (i) while by $\Delta_{15} - k_{pe} v$ and $\Delta_{15} - \Delta_{12} + k_{ce} v$ in case (ii) with largely reduced effective wavevectors $k_{pe} = k_p - k_a$ and $k_{ce} = k_{c1} - k_{c2}$, which must result in well suppressed Doppler broadenings on two-photon transitions. On the other hand, the four-photon detuning should be replaced by $\Delta_{12} + (k_{pe} - k_{ce})v$ in case (i) while by $\Delta_{12} - (k_{pe} + k_{ce})v$ in case (ii). Hence, it is

Doppler-free and velocity-dependent, respectively, in cases (i) and (ii) due to $k_{pe} = k_{ce}$ with $k_p = k_{c1}$ and $k_a = k_{c2}$, which is crucial for realizing the transmission non-reciprocity of a weak probe field.

It is worth noting that same results can be attained in other two cases where the travelling directions of probe, assistant, and coupling fields are all reversed as compared to cases (i) and (ii), respectively. In the remaining twelve cases, however, Doppler broadenings on one or both two-photon transitions will be greatly enhanced so that the original five-level Λ system cannot be treated as a reduced three-level Λ system again by eliminating states $|3\rangle$ and $|4\rangle$ via large single-photon detunings. Consequently, the transmission of a probe field does not depend critically on its travelling direction and we cannot attain broadband and tunable transmission non-reciprocity in the absence of largely narrowed Doppler broadenings.

With above considerations, it is viable to calculate the mean populations in state $|5\rangle$ by making following integrations for the two cases of our interest

$$\rho_{55}^{\pm} = \int \mathrm{d}v f(v)\, \rho_{55}\left(\pm k_p v, \mp k_a v; k_{c1} v, -k_{c2} v\right), \tag{3}$$

where $f(v) = e^{-v^2/v_p^2}/(v_p\sqrt{\pi})$ denotes the Maxwell velocity distribution with $v_p = \sqrt{2k_BT/M}$ being the most probable atomic velocity, k_B the Boltzmann constant, T the atomic temperature, and M the atomic mass. With $\rho_{55}^{\pm}$ in hand, we can further calculate the absorption coefficients and the probe transmissivities via

$$\alpha_p^{\pm} = \frac{Nd_{13}^2}{\hbar\varepsilon_0}\frac{\pi\Gamma}{\lambda_p}\frac{\rho_{55}^{\pm}}{|\Omega_p|^2}, \tag{4a}$$

$$T_p^{\pm} = e^{-\alpha_p^{\pm}L}, \tag{4b}$$

which should be direction-dependent due to $\rho_{55}^{+} \neq \rho_{55}^{-}$. In addition to the qualitative evaluations via $T_p^{+} \neq T_p^{-}$, the transmission non-reciprocity for a probe field can also be quantified via two figure of merits

$$\mathtt{IR} = 10\log_{10}\left(\frac{T_p^{+}}{T_p^{-}}\right), \tag{5a}$$

$$\mathtt{IL} = -10\log_{10} T_p^{+}, \tag{5b}$$

referring to isolation ratio and insertion loss, respectively. Here we have considered that $T_p^{+} \gg T_p^{-}$ around the four-photon resonance $\Delta_{12} + \Delta_{2d} = 0$ where a two-photon EIT window can be found in case (i) due to the Doppler-free arrangement but is smeared out in case (ii) by the residual Doppler effect. Below, we will adopt $\mathtt{IR} > 20$ dB (i.e. $T_p^{+}/T_p^{-} > 100$) and $\mathtt{IL} < 1.0$ dB (i.e. $T_p^{+} > 0.794$) as two basic criteria for realizing a high-performance isolator based on the transmission non-reciprocity.

It is worth noting that, effective Rabi frequencies and dynamic Stark shifts in the reduced three-level Λ system are also velocity-dependent as shown below

$$\Omega_{pe}^{\pm} = -\frac{\Omega_p\Omega_a}{\Delta_p \pm k_p v}, \tag{6a}$$

$$\Omega_{ce}^{\pm} = -\frac{\Omega_{c1}\Omega_{c2}}{\Delta_{c2} - k_{c2} v}, \tag{6b}$$

$$\Delta_{2d}^{\pm} = -\frac{|\Omega_{c1}|^2}{\Delta_{c1} + k_{c1} v}, \tag{6c}$$

$$\Delta_{5d}^{\pm} = \frac{|\Omega_a|^2}{\Delta_a \mp k_a v} + \frac{|\Omega_{c2}|^2}{\Delta_{c2} - k_{c2} v}, \tag{6d}$$

which may destroy the two-photon EIT effect in case (i). Fortunately, their values are very small and more importantly change little for most atomic velocities even at a room temperature as we choose large enough $|\Delta_{p,a,c1,c2}|$. Last but not least, the assistant (second coupling) field may intersect the oppositely propagating probe (first coupling) field with a misaligned angle $180^\circ - \theta$ while the latter is kept to always travel along the $\pm z$ (z) direction with '+' and '−' referring to cases (i) and (ii), respectively. Then, wavevectors $k_{a,c2}$ should be replaced with the effective ones $k_{a,c2}^{\mathtt{eff}} = k_{a,c2}\cos(180^\circ - \theta)$ in calculating $\rho_{55}^{\pm}$. The velocity-insensitive $\{\Omega_{pe,ce}^{\pm}, \Delta_{2d,5d}^{\pm}\}$ and angle-dependent $k_{a,c2}^{\mathtt{eff}}$ can be explored to bring additional degrees of dynamic manipulation on the transmission non-reciprocity discussed in the next two sections.

Finally, we note that the two coupling fields suffer little absorption because $\rho_{55,22} \to 0$ and $\rho_{11} \to 1$ in the limit of $\Omega_{pe} \ll \Omega_{ce}$. The assistant field also suffers little absorption because $\Omega_p \ll \Omega_a$ and the loss of a $\hbar\omega_a$ photon must be accompanied by the loss of a $\hbar\omega_p$ photon. That is, the assistant field is not significantly attenuated even if the probe field has been totally absorbed. Hence, their negligible attenuation during propagation will not comprise the probe field's isolation ratio and insertion loss.

3. Broadband non-reciprocity

In this section, we examine via numerical calculations the broadband transmission non-reciprocity of a probe field incident upon a sample of thermal ^{87}Rb atoms driven into the five-level Λ configuration in figure 1(a) equivalent to the three-level Λ configuration in figure 1(b) with dominant two-photon transitions. Half Doppler broadenings can be estimated by $\delta\omega_D = \sqrt{\ln 2}v_p/\lambda_i$ and are about 250 (274) MHz on the lower (upper) single-photon transitions with $i \in \{p, c1\}$ ($i \in \{a, c2\}$) but reduced to 22.8 MHz on the two-photon transitions with $i \in \{pe, ce\}$ at the temperature $T \simeq 300$ K ($v_p \simeq 240$ m s^{-1}). It is hence appropriate to choose $\Delta_{a,c1}/ \simeq -\Delta_{p,c2} \simeq 1000$ MHz and $\Omega_{a,c1,c2} \lesssim 50$ MHz so that the single-photon transitions can be neglected for all atomic velocities while the two-photon transitions are kept near resonances by setting $\Delta_{15} \simeq 0$ and $\Delta_{15} - \Delta_{12} - \Delta_{12d} \simeq 0$ with Δ_{12d} being small and Δ_{15d} negligible (due to $\Delta_a = -\Delta_{c2}$).

In figure 2, we plot two-photon absorption coefficients $\alpha_p^{\pm}$ as functions of probe detuning Δ_p for three typical temperatures spanning a wide range. We can see from figures 2(a$_1$) and (a$_2$) that there exist no observable differences between α_p^+ and α_p^- at a low enough temperature $T = 1.0$ mK, leaving the cold atomic sample reciprocal in absorption to a weak probe field incident from the left or right side. Moreover, it is clear that each absorption spectrum of α_p^+ and α_p^- on the two-photon transition $|1\rangle \leftrightarrow |5\rangle$ exhibits a typical EIT doublet with an in-between dip at $\Delta_p \simeq -\Delta_a$, which can be attributed as usual to the quantum destructive interference generated by an effective coupling field Ω_{ce} acting upon the two-photon transition $|2\rangle \leftrightarrow |5\rangle$. As the temperature increases to $T = 10$ K in figures 2(b$_1$) and (b$_2$) or to $T = 300$ K in figures 2(c$_1$) and (c$_2$), we find that α_p^+ and α_p^- become evidently different around $\Delta_p \simeq -\Delta_a$ where the two-photon EIT dips remain unchanged in depth, though become narrower, for α_p^+ but entirely disappear for α_p^-. The underlying physics is related to the four-photon detunings

$$\Delta_{12}^{\pm} = \Delta_{12} + \left(k_{ep} \mp k_{ec}\right) v - \Delta_{2d}^{\pm}, \tag{7}$$

for $\alpha_p^{\pm}$ with $\Delta_{2d}^+ = \Delta_{2d}^-$ depending on but not sensitive to v. This equation indicates that α_p^+ is roughly Doppler-free around $\Delta_{12} = 0$ due to $k_{ep} - k_{ec} = 0$ so that the EIT window remains perfect while α_p^- is velocity-dependent everywhere due to $k_{ep} + k_{ec} = 2k_{ep}$ so that the EIT window entirely disappears. It is worth noting that the increase of $\alpha_p^{\pm}$ with Ω_{pe} observed for all three temperatures is a feature absent in the three-level Λ system dominated by single-photon transitions and will be used later to manipulate the transmission non-reciprocity.

Above results indicate that the forward probe field can exhibit a rather high transmissivity, while the backward probe field will be strongly absorbed, around the four-photon resonance $\Delta_p + \Delta_a \simeq \Delta_{c1} + \Delta_{c2}$ in a sample of thermal atoms described by $\alpha_p^{\pm}$. Such an evident transmission non-reciprocity, enabling an efficient optical isolation, has been numerically examined in figure 3 in terms of transmissivities $T_p^{\pm}$, isolation ratio `IR`, and insertion loss `IL` as functions of probe detuning Δ_p. We find from figure 3(a) that T_p^+ approaches unity with a transmission bandwidth of the order of MHz determined here by the effective coupling Rabi frequency Ω_{ce} while figure 3(b) shows that T_p^- remains low in a much wider range though decreases slowly as $|\Delta_p|$ becomes smaller due to an increase of the effective probe Rabi frequency Ω_{pe}. It is also clear from figures 3(c) and (d) that `IR` could reach the maximum of 22.5 dB while `IL` might be as low as 0.3 dB, indicating the possibility for achieving a high-performance optical isolator. Note however that the effective coupling Rabi frequency Ω_{ce} should not be too small, otherwise the insertion loss will exceed 1.0 dB on one hand and the non-reciprocal transmission bandwidth will reduce to be invisible on the other hand (not shown).

We are committed in particular to achieving the nonreciprocal transmission of a controlled broad bandwidth based on thermal atoms dominated by two-photon transitions under consideration here. Working in the regime of near-resonant two-photon and four-photon transitions, the single-photon detunings can be tuned in a relatively wide range yet without changing too much the four important quantities plotted in figure 4, which then facilitates the essential WDM function in an all-optical network. This has been examined by modulating $\Delta_p = -\Delta_a$ in the range of $\{-1200, -800\}$ MHz to ensure that two-photon transitions are dominant over single-photon transitions. In this range, it is found that slight changes of effective Rabi frequency Ω_{pe} has resulted in the evident changes in $T_p^{\pm}$, `IR`, and `IL`, which is

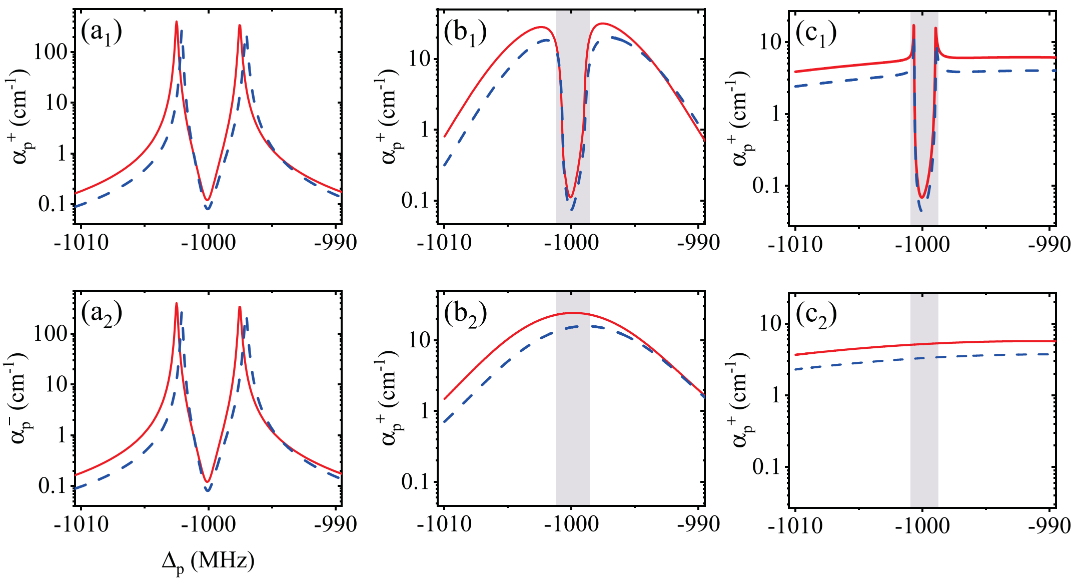

Figure 2. Absorption coefficients α_p^+ (upper) and α_p^- (lower) as functions of probe detuning Δ_p with $T = 1.0$ mK (a_1), (a_2), 10 K (b_1), (b_2), and 300 K (c_1), (c_2) for $\Omega_a = 50$ MHz (red-solid) and 40 MHz (blue-dashed). Other parameters are $\Omega_p = 0.1$ MHz, $\Omega_{c1} = \Omega_{c2} = 50$ MHz, $\Delta_a = \Delta_{c1} = 1000$ MHz, $\Delta_{c2} = -1002.5$ MHz, $\Gamma_{53} = \Gamma_{54} = 0.19$ MHz, $\gamma_l = 0.05$ MHz, $\gamma_{21} = 2.0$ kHz, $\theta = 180°$, $N = 2.0 \times 10^{12}$ cm^{-3}, $L = 1.0$ cm, $\lambda_p = 795.0$ nm, and $d_{13} = 2.537 \times 10^{-29}$ Cm.

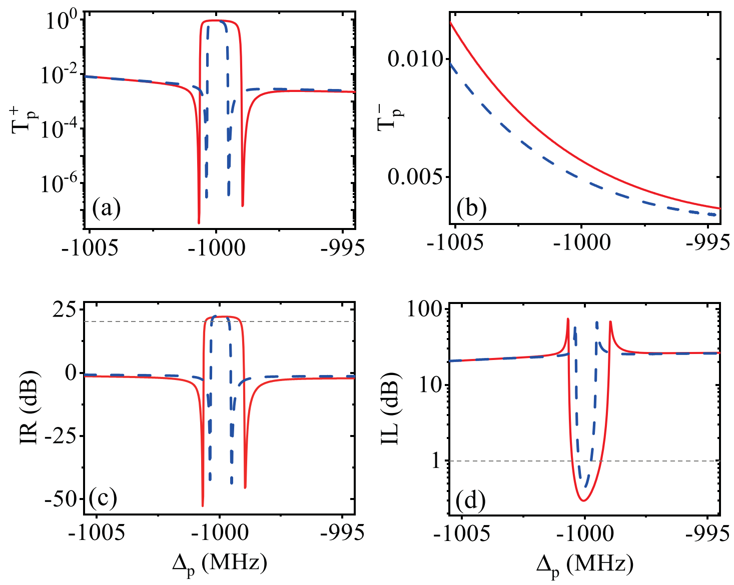

Figure 3. Probe transmissivities T_p^+ (a) and T_p^- (b) as well as isolation ratio IR (c) and insertion loss IL (d) against probe detuning Δ_p for $\Omega_{c1} = \Omega_{c2} = 50$ MHz (red-solid) and 40 MHz (blue-dashed). Other parameters are the same as in figure 2 except $T = 300$ K and $\Omega_a = 50$ MHz. Gray dotted lines refer to IR = 20 dB in (c) or IL = 1.0 dB in (d) as a reference.

impossible in a typical three-level Λ system. More importantly, figure 4 shows that the isolation ratio of IR > 20 dB and the insertion loss of IL < 1.0 dB can be attained in a wide frequency range of $150 \sim 250$ MHz, indicating that it is viable to achieve the nonreciprocal transmission by simultaneously handling tens of light signals with different frequencies. Figure 5 further shows that the nonreciprocal transmission exhibits a maximal bandwidth up to 1.4 GHz with IR > 20 and IL < 1.0 dB as we choose $\theta = 158°$ so as to have the smallest Doppler broadenings on both two-photon transitions $|1\rangle \leftrightarrow |5\rangle$ and $|2\rangle \leftrightarrow |5\rangle$. This big enlargement of nonreciprocal bandwidth can be understood by resorting to numerical results shown in the next section.

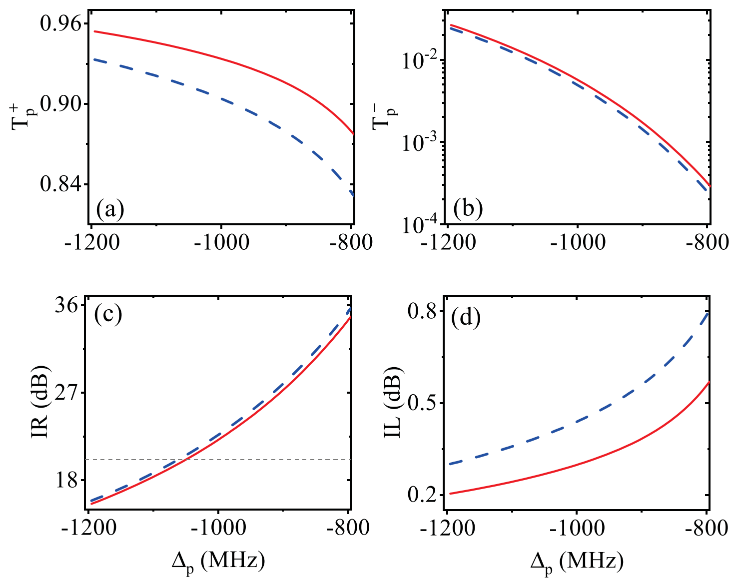

Figure 4. Probe transmissivities T_p^+ (a) and T_p^- (b) as well as isolation ratio IR (c) and insertion loss IL (d) against probe detuning Δ_p for $\Omega_{c1} = \Omega_{c2} = 50$ MHz (red-solid) and 40 MHz (blue-dashed). Other parameters are the same as in figure 3 except $\Delta_a = -\Delta_p$. Gray dotted lines refer to IR = 20 dB in (c) or IL = 1.0 dB in (d) as a reference.

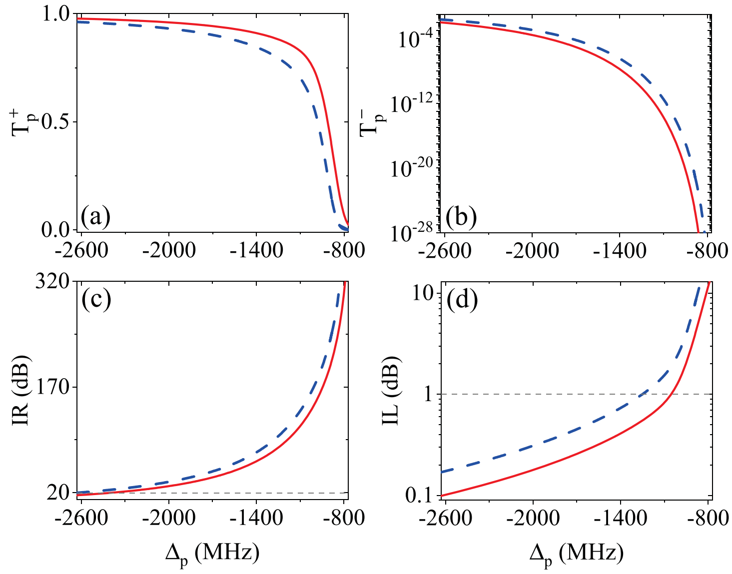

Figure 5. Probe transmissivities T_p^+ (a) and T_p^- (b) as well as isolation ratio IR (c) and insertion loss IL (d) against probe detuning Δ_p for $\Omega_{c1} = \Omega_{c2} = 50$ MHz (red-solid) and 40 MHz (blue-dashed). Other parameters are the same as in figure 4 except $\theta = 158^\circ$. Gray dotted lines refer to IR = 20 dB in (c) or IL = 1.0 dB in (d) as a reference.

4. Nonreciprocal tunability

In this section, we examine two flexible ways for manipulating the transmission non-reciprocity by modulating additional parameters, Rabi frequency Ω_a and misaligned angle θ, to gain further insights into nonreciprocal optical responses. This is intrinsic to the reduced three-level Λ system dominated by two-photon near-resonant transitions and expected to facilitate the signal or information processing in an all-optical network.

First, we plot in figure 6 probe transmissivities $T_p^{\pm}$ together with isolation ratio IR and insertion loss IL against Rabi frequency Ω_a of the assistant field. It is easy to see from figures 6(a) and (b) that a large variation of Ω_a in the range of $\{0, 60\}$ MHz, corresponding to a small variation of Ω_{pe} in the range of $\{0, 6\}$ kHz, will result in the evident variations of $T_p^{\pm}$, which cannot be attained in a typical three-level Λ system since it is independent of probe Rabi frequency Ω_p. We should note, however, that T_p^+ just reduces a few percentage from 1.0 to 0.90 or 0.86 (depending on coupling Rabi frequencies $\Omega_{c1} = \Omega_{c2}$) while T_p^- suffers a much

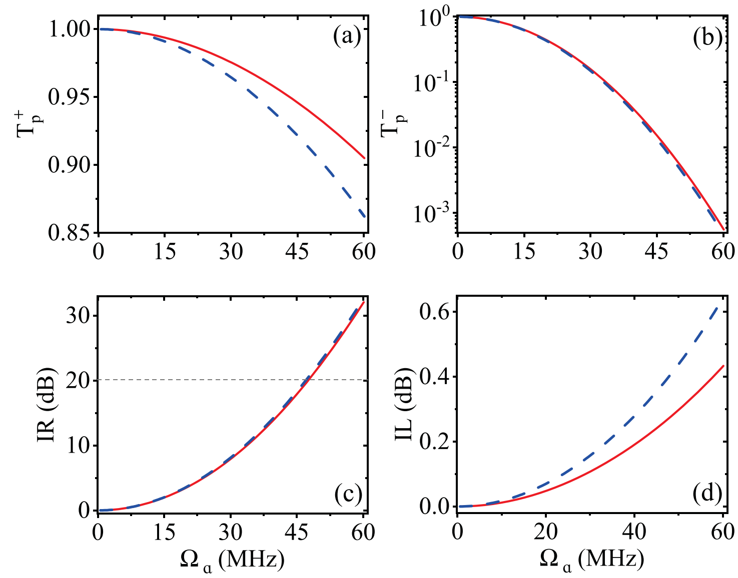

Figure 6. Probe transmissivities T_p^+ (a) and T_p^- (b) as well as isolation ratio $\mathtt{IR}$ (c) and insertion loss $\mathtt{IL}$ (d) against Rabi frequency Ω_a for $\Omega_{c1} = \Omega_{c2} = 50$ MHz (red-solid) and 40 MHz (blue-dashed). Other parameters are the same as in figure 3 except $\Delta_p = -1000$ MHz. Gray dotted lines refer to $\mathtt{IR} = 20$ dB in (c) or $\mathtt{IL} = 1.0$ dB in (d) as a reference.

sharper reduction from 1.0 to 5×10^{-4} or 4×10^{-4} (less sensitive to the change of $\Omega_{c1} = \Omega_{c2}$). Accordingly, we find from figures 6(c) and (d) that isolation ratio $\mathtt{IR}$ increases faster than insertion loss $\mathtt{IL}$ with the increase of Ω_a, and we can achieve $\mathtt{IR} > 20$ dB only with $\Omega_a > 47.5$ MHz ($\Omega_a > 47.0$ MHz) while $\mathtt{IL} < 1.0$ dB holds for $\Omega_a \leqslant 60$ MHz no matter $\Omega_{c1} = \Omega_{c2} = 50$ MHz or $\Omega_{c1} = \Omega_{c2} = 40$ MHz. It is also clear that the assistant field should be carefully modulated in order to ensure an ideal trade-off between $\mathtt{IR}$ and $\mathtt{IL}$, relevant to a high-performance optical isolator, with the working range of Ω_a depending on $\Omega_{c1} = \Omega_{c2}$ for a fixed Ω_p.

Then, we try to plot in figure 7 probe transmissivities $T_p^{\pm}$ together with isolation ratio $\mathtt{IR}$ and insertion loss $\mathtt{IL}$ against misaligned angle θ between wavenumbers k_p (k_{c1}) and $-k_a$ ($-k_{c2}$) in the case of $\Delta_p = -\Delta_a$. Figure 7(a) shows that T_p^+ decreases slowly above a quite high value until θ reduces from 180° to 157.3°, while approaches quickly 4×10^{-3} (5×10^{-6}) for $\Omega_{c1} = \Omega_{c2} = 50$ MHz ($\Omega_{c1} = \Omega_{c2} = 40$ MHz) as θ further reduces from 157.3° to 156.5°. Figure 7(b) shows instead that T_p^- exhibits an extremely small minimum around $\theta = 157.3°$, decreases more evidently as θ reduces from 180° to 157.3°, and increases surprisingly back to 1.0 as θ further reduces from 157.3° to 156.5°. The joint variations of T_p^+ and T_p^- due to an effective control of Doppler broadenings on two-photon transitions by modulating angle θ then lead to the results shown in figures 7(c) and (d), where $\mathtt{IR}$ exhibits a very large maximum at $\theta = 157.3°$ while $\mathtt{IL}$ increases continuously to a saturation value as θ reduces to 156.5°. It is worth noting that the critical requirements of $\mathtt{IR} > 20$ dB and $\mathtt{IL} < 1.0$ dB could be simultaneously attained only with $\theta > 158.6°$ ($\theta > 160.3°$) for $\Omega_{c1} = \Omega_{c2} = 50$ MHz ($\Omega_{c1} = \Omega_{c2} = 40$ MHz), while the maximum of $\mathtt{IR}$ at $\theta = 157.3°$ is meaningless as the corresponding $\mathtt{IL}$ is too large. Anyway, we can get a better trade-off between $\mathtt{IR}$ and $\mathtt{IL}$ for realizing a high-performance optical isolation by modulating θ in the range of $\{157.3°, 180°\}$.

To better understood what are observed in figure 7, we examine in figure 8 absorption coefficients $\alpha_p^{\pm}$ as functions of probe detuning Δ_p for three typical values of angle θ. Figure 8(a) shows that the EIT window of α_p^+ becomes shallower and shallower and meanwhile more and more asymmetric as θ gradually reduces. Figure 8(b) shows that α_p^- changes in a way similar to α_p^+ as far as their spectral widths are concerned, i.e. both become narrower as θ gradually reduces. An evident change of α_p^- different from α_p^+ lies in that the two-photon EIT dip is absent for both $\theta = 180°$ and $\theta = 160°$ but can be observed like α_p^+ for $\theta = 156.5°$. This can be understood by considering that $\theta = 156.5°$ corresponds to the case where both two-photon transitions $|1\rangle \leftrightarrow |5\rangle$ and $|2\rangle \leftrightarrow |5\rangle$ become Doppler free due to $k_{p,c1} = k_{a,c2}^{\mathtt{eff}}$ so that it is impossible to attain the transmission non-reciprocity around four-photon resonance without residual Doppler broadenings. As to the asymmetric features of α_p^+ and α_p^- spectra, they arise in fact from effective Rabi frequencies $\Omega_{pe}^{\pm}$ and $\Omega_{ce}^{\pm}$ as well as dynamic Stark shifts $\Delta_{2d}^{\pm}$ and $\Delta_{5d}^{\pm}$, whose velocity dependence cannot be eliminated via appropriate arrangements of the probe, assistant, and coupling fields. Fortunately, the four quantities exhibit quite small values and change just a little for different atomic velocities so that the EIT dip remains well developed. With above discussions, we conclude that the quenching of T_p^+ for $\theta < 157.3°$ and the minimum

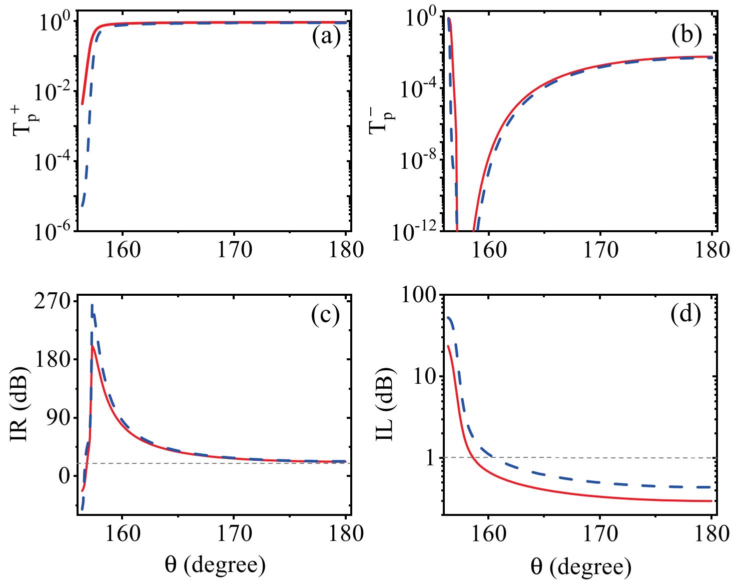

Figure 7. Probe transmissivities T_p^+ (a) and T_p^- (b) as well as isolation ratio $\mathtt{IR}$ (c) and insertion loss $\mathtt{IL}$ (d) against angle θ for $\Omega_{c1} = \Omega_{c2} = 50$ MHz (red-solid) and 40 MHz (blue-dashed). Other parameters are the same as in figure 3 except $\Delta_p = -1000$ MHz. Gray dotted lines refer to $\mathtt{IR} = 20$ dB in (c) or $\mathtt{IL} = 1.0$ dB in (d) as a reference.

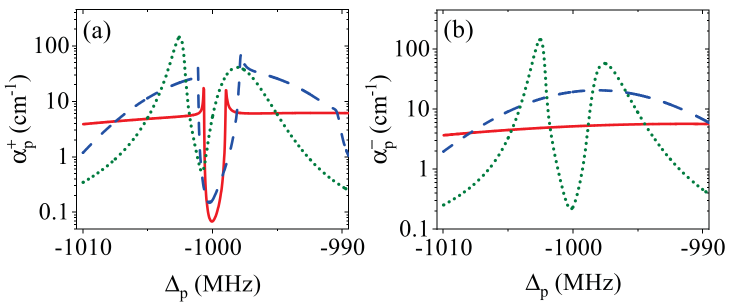

Figure 8. Absorption coefficients α_p^+ (a) and α_p^- (b) as functions of probe detuning Δ_p for $T = 300$ K with $\theta = 180°$ (red-solid), 160° (blue-dashed), and 156.5° (green-dotted). Other parameters are the same as in figure 3.

of T_p^- at $\theta = 157.3°$ in figure 7 arise from the Doppler-free asymmetric EIT spectra of $\alpha_p^\pm$ and a slight velocity-dependent shift of the EIT dip away from four-photon resonance.

What we observe in figures 7 and 8 answer why the nonreciprocal bandwidth can be greatly enlarged by replacing $\theta = 180°$ with $\theta = 158°$ at $T = 300$ K as shown in figure 5. Finally, we examine in figure 9 the joint effects of angle θ and temperature T on the transmission non-reciprocity in terms of isolation ratio $\mathtt{IR}$ and insertion loss $\mathtt{IL}$ in the case of $\Delta_p = -\Delta_a$. We can see from figure 9(a) that the maximum of $\mathtt{IR}$ (~ 150 dB) moves slowly from $T \simeq 2.5$ K to $T \simeq 7.0$ K as θ decreases from 180° to 165°, but turns to move quickly toward $T \simeq 13$ K, $T \simeq 39$ K, and $T \simeq 147$ K as θ further decreases to 162.5°, 160°, and 158°, respectively. Figure 9(b) shows that $\mathtt{IL}$ always decreases slowly as T increases in the visible range for $\theta \gtrsim 162.5°$ and remains well below 0.5 dB, but starts to increase quickly as T increases to be high enough for $\theta \lesssim 162.5°$ and may far exceed 1.0 dB. These findings can be attributed to the fact that, since T and θ together determine Doppler broadenings, the same change of Doppler broadenings resulted from the same change of θ requires a larger change of T as θ approaches the critical value 157.3° referring to vanishing Doppler broadenings. To conclude, this figure tells that it is viable to attain a better trade-off between $\mathtt{IR}$ and $\mathtt{IL}$ for realizing a high-performance optical isolator by modulating both θ and T in appropriate ranges. The main benefit of such a joint modulation lies in that it promises a flexible manipulation on both residual Doppler broadenings of two-photon transitions and inevitable Doppler shifts of effective Rabi frequencies and dynamic Stark shifts.

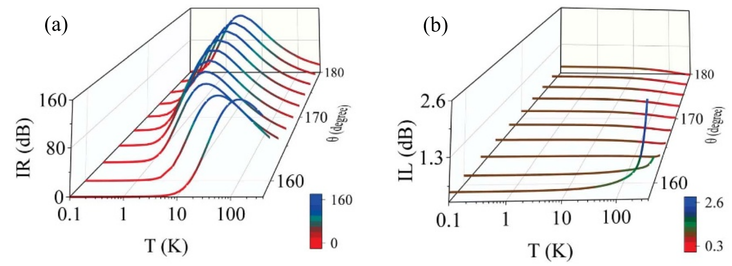

Figure 9. Isolation ratio IR (a) and insertion loss IL (b) against temperature T and angle θ. Relevant parameters are the same as in figure 3 except $\Delta_p = -1000$ MHz.

Table 1. Basic requirement, influence of parameters Ω_a, θ, and T, and main conclusion.

Basic requirement:	$\Omega_c = 40 \sim 50$ MHz, $\Delta_{c2} \simeq -\Delta_{c1} = -1000$ MHz, and $\Delta_p = -\Delta_a \lesssim -800$ MHz for attaining a large non-reciprocal transmission bandwidth ($\sim$200 MHz for $\theta = 180^\circ$ while ~ 1.4 GHz for $\theta = 158^\circ$).
Influence of Ω_a:	An increase of Ω_a results in an increase of both IR and IL so that the transmission non-reciprocity characterized by IR > 20 dB and IL < 1.0 dB can be attained only for moderate values of Ω_a.
Influence of θ:	A decrease of θ from 180° to $\sim 160^\circ$ can be explored to attain a high-performance optical isolation for a certain value of $\Delta_p = -\Delta_a$ by increasing IR from 20 dB while leaving IL below 1.0 dB.
Influence of T:	The optimal value of T corresponding to the maximum of IR ($\sim$150 dB) increases first slowly and then quickly from 2.5 K to 147 K with IL keeping below 1.0 dB as θ reduces from 180° to 158°.
Main conclusion:	It is viable to optimize the transmission non-reciprocity with a large tunable bandwidth via a joint variation of parameters Ω_a, θ, and T in order to attain a better trade-off between IR and IL.

5. Conclusions

In summary, we have investigated an efficient scheme for achieving the magnet-free optical non-reciprocity in a three-level Λ system dominated by two-photon transitions by considering free-space thermal ^{87}Rb atoms. The forward probe field is found to experience a Doppler-free EIT window and hence suffers very low losses in transmission, while the backward probe field is strongly absorbed because the EIT window is smeared out as the Doppler shifts on two-photon transitions $|1\rangle \leftrightarrow |5\rangle$ and $|2\rangle \leftrightarrow |5\rangle$ do not cancel out again. It is of particular interest that the non-reciprocal transmission may be well controlled by modulating the frequency and amplitude of an assistant field as well as a common misaligned angle between the two pairs of $\{\omega_p, \omega_a\}$ and $\{\omega_{c1}, \omega_{c2}\}$ fields. It is also important that this transmission non-reciprocity can exhibit high isolation ratios and low insertion losses in a wide frequency range, benefiting from largely reduced Doppler broadenings on two-photon transitions $|1\rangle \leftrightarrow |5\rangle$ and $|2\rangle \leftrightarrow |5\rangle$. That means, our scheme allows to manipulate hundreds of probe fields as multiple light signals at the same time with similar isolation ratios and insertion losses due to their insensitivities to single-photon detunings and hence facilitate WDM applications in all-optical networks. The most important figures of merit in our present work are summarized in table 1.

Data availability statement

All data that support the findings of this study are included within the article (and any supplementary files).

Acknowledgments

This work is supported by the National Natural Science Foundation of China (Nos. 62375047 and 12074061).

Appendix A. Hamiltonians and dynamic equations

For the five-level Λ system under consideration, we can write down the interaction Hamiltonian

$$H_I = -\hbar \begin{pmatrix} 0 & 0 & \Omega_p^* & 0 & 0 \\ 0 & \Delta_{12} & 0 & \Omega_{c1}^* & 0 \\ \Omega_p & 0 & \Delta_{13} & 0 & \Omega_a^* \\ 0 & \Omega_{c1} & 0 & \Delta_{14} & \Omega_{c2}^* \\ 0 & 0 & \Omega_a & \Omega_{c2} & \Delta_{15} \end{pmatrix}, \tag{A.1}$$

with $\Delta_{12} = \Delta_p + \Delta_a - \Delta_{c1} - \Delta_{c2}$, $\Delta_{13} = \Delta_p$, $\Delta_{14} = \Delta_p + \Delta_a - \Delta_{c2}$, and $\Delta_{15} = \Delta_p + \Delta_a$.

Working in the regime of $\Delta_p + \Delta_a \simeq 0$, $\Delta_{c1} + \Delta_{c2} \simeq 0$, $|\Delta_{p,a}| \gg \Omega_{p,a}$, and $|\Delta_{c1,c2}| \gg \Omega_{c1,c2}$, the five-level Λ system can be reduced to a three-level Λ system by eliminating intermediate states $|3\rangle$ and $|4\rangle$. Then, it is viable to derive through the time-averaged adiabatic-elimination method [50] the effective Hamiltonian

$$H_e = -\hbar \begin{pmatrix} 0 & 0 & \Omega_{pe}^* \\ 0 & \Delta_{12} + \Delta_{2d} & \Omega_{ce}^* \\ \Omega_{pe} & \Omega_{ce} & \Delta_{15} + \Delta_{5d} \end{pmatrix}, \tag{A.2}$$

where we have introduced a new Rabi frequency $\Omega_{pe} = -\Omega_p\Omega_a/\Delta_p$ ($\Omega_{ce} = -\Omega_{c1}\Omega_{c2}/\Delta_{c2}$) for the effective probe (coupling) field of frequency $\omega_{pe} = \omega_p + \omega_a$ ($\omega_{ce} = \omega_{c1} + \omega_{c2}$) acting upon the two-photon near-resonant transition $|1\rangle \leftrightarrow |5\rangle$ ($|2\rangle \leftrightarrow |5\rangle$). Note also that $\Delta_{2d} \simeq -|\Omega_{c1}|^2/\Delta_{c1}$ ($\Delta_{5d} \simeq |\Omega_a|^2/\Delta_a + |\Omega_{c2}|^2/\Delta_{c2}$) describes the dynamic Stark shift of state $|2\rangle$ ($|5\rangle$) as a direct result of the virtual absorption and emission of ω_{c1} (ω_a and ω_{c2}) photons, which will result in a slight deviation of the four-photon (two-photon) resonance from $\Delta_{12} = 0$ ($\Delta_{15} = 0$).

For simplicity, below we just write down the dynamic equations of density matrix elements ρ_{mn} for the reduced three-level Λ system starting from equation (A.2)

$$\partial_t\rho_{22} = \Gamma_{52}\rho_{55} + i\Omega_{ce}^*\rho_{52} - i\Omega_{ce}\rho_{25}, \tag{A.3a}$$
$$\partial_t\rho_{11} = \Gamma_{51}\rho_{55} + i\Omega_{pe}^*\rho_{51} - i\Omega_{pe}\rho_{15}, \tag{A.3b}$$
$$\partial_t\rho_{52} = -g_{52}\rho_{52} + i\Omega_{pe}\rho_{12} + i\Omega_{ce}(\rho_{22} - \rho_{55}), \tag{A.3c}$$
$$\partial_t\rho_{51} = -g_{51}\rho_{51} + i\Omega_{ce}\rho_{21} + i\Omega_{pe}(\rho_{11} - \rho_{55}), \tag{A.3d}$$
$$\partial_t\rho_{21} = -g_{21}\rho_{21} + i\Omega_{ce}^*\rho_{51} - i\Omega_{pe}\rho_{25}, \tag{A.3e}$$

which are restricted by $\rho_{ij} = \rho_{ji}^*$ and $\rho_{11} + \rho_{22} + (1 + \eta_{53} + \eta_{54})\rho_{55} = 1$ with $\eta_{53}\rho_{55} = \Gamma_{53}/(\Gamma_{31} + \Gamma_{32})\rho_{55}$ and $\eta_{54}\rho_{55} = \Gamma_{54}/(\Gamma_{41} + \Gamma_{42})\rho_{55}$ accounting for populations in states $|3\rangle$ and $|4\rangle$, respectively, due to the inevitable spontaneous decay. Above, we have defined the complex decoherence rates $g_{52} = \gamma_{52} + i(\Delta_{15} - \Delta_{12} + \Delta_{5d} - \Delta_{2d})$, $g_{51} = \gamma_{51} - i(\Delta_{15} + \Delta_{5d})$ and $g_{21} = \gamma_{21} - i(\Delta_{12} + \Delta_{2d})$ after including the dynamic Stark shifts Δ_{2d} and Δ_{5d}. Typically, the real dephasing rate γ_{mn} of coherence ρ_{mn} depends on the spontaneous decay rates Γ_{mk} and Γ_{nk} of populations ρ_{mm} and ρ_{nn} through $\gamma_{mn} = \sum_k(\Gamma_{mk} + \Gamma_{nk})/2$. We have also defined $\Gamma_{51} = \Gamma_{31}\eta_{53} + \Gamma_{41}\eta_{54}$ and $\Gamma_{52} = \Gamma_{32}\eta_{53} + \Gamma_{42}\eta_{54}$ as the effective decay rates from state $|5\rangle$ to states $|1\rangle$ and $|2\rangle$, respectively.

Appendix B. Absorption coefficient

Here, we try to derive the two-photon absorption coefficient of a probe field based on population ρ_{55} in state $|5\rangle$ as the five-level Λ system in figure 1(a) reduces to the three-level Λ system in figure 1(b). To this end, we first note that the probe field exhibits an intensity defined as $I_p = c\epsilon_0 E_p^2/2 = 2\hbar^2 c\epsilon_0|\Omega_p|^2/d_{13}^2$. Then, the number of probe photons, passing through a section of the atomic sample at position z, per time is given by

$$\frac{N_p(z)}{\mathrm{d}t} = \frac{\pi r_p^2}{\hbar\omega_p} I_p(z) = \frac{\hbar\epsilon_0\lambda_p r_p^2}{d_{13}^2}|\Omega_p(z)|^2, \tag{B.1}$$

where r_p denotes the probe beam radius. With this consideration, we can further attain the number of photons lost per time in an atomic slice from z to $z + \mathrm{d}z$

$$\frac{\mathrm{d}N_p}{\mathrm{d}t} = \frac{\hbar c\epsilon_0\lambda_p r_p^2}{d_{13}^2}\mathrm{d}I_p, \tag{B.2}$$

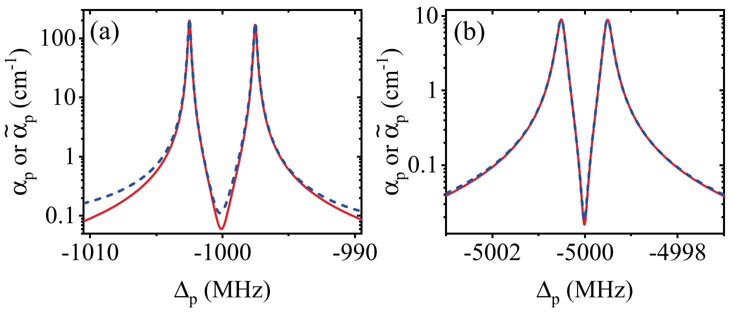

Figure B1. Absorption coefficients α_p (red-solid) and $\tilde{\alpha}_p$ (blue-dashed) as functions of probe detuning Δ_p with $\Delta_a = \Delta_{c1} = 1000$ MHz (a) and $\Delta_a = \Delta_{c1} = 5000$ MHz (b). Other parameters are the same as in figure 2 except $\Omega_a = 50$ MHz and $\Delta_{c2} = -\Delta_{c1} - \Delta_{5d} + \Delta_{2d}$ changes with $\Delta_a = \Delta_{c1}$.

with $\mathrm{d}N_p = N_p(z+\mathrm{d}z) - N_p(z)$ and $\mathrm{d}I_p = |\Omega_p(z+\mathrm{d}z)|^2 - |\Omega_p(z)|^2$. Meanwhile, the number of atoms in state $|5\rangle$ lost per time, due to spontaneous decay after absorbing probe photons, in this atomic slice is given by

$$\frac{\delta n_a}{\mathrm{d}t} = N\pi r_p^2 \rho_{55} \Gamma \mathrm{d}z, \tag{B.3}$$

where we have considered that the probe field interacts with $N\pi r_p^2 \mathrm{d}z$ atoms in this slice of density N.

According to the requirement of energy conservation $\mathrm{d}N_p/\mathrm{d}t = -\delta n_a/\mathrm{d}t$, we can derive the probe transmissivity for an atomic sample of length L

$$T_p = \frac{I_p(L)}{I_p(0)} = \left|\frac{\Omega_p(L)}{\Omega_p(0)}\right|^2 = e^{-\alpha_p L}, \tag{B.4}$$

with the absorption coefficient being

$$\alpha_p = \frac{N d_{13}^2}{\hbar \epsilon_0} \frac{\pi \Gamma}{\lambda_p} \frac{\rho_{55}}{|\Omega_p|^2}, \tag{B.5}$$

which should be Ω_p-independent since $\rho_{55} \propto |\Omega_p|^2$ in the limit of a weak probe field. It is worth noting that the absorption coefficient may also be expressed as

$$\tilde{\alpha}_p = \frac{N d_{13}^2}{\hbar \epsilon_0} \frac{2\pi}{\lambda_p} \frac{\mathrm{Im}\rho_{31}}{\Omega_p}, \tag{B.6}$$

with $\rho_{31} \propto \Omega_p$ obtained by solving density matrix equations of the original five-level Λ system in the steady state. Equations (B.5) and (B.6) allow us to examine the validity of a reduced three-level Λ system by presenting a numerical comparison between the two absorption coefficients with appropriate parameters as shown in figure B1. The results tell that absorption coefficients α_p and $\tilde{\alpha}_p$ are in good agreement for $|\Delta_{a,c1,c2}|/\Omega_{a,c1,c2} = 20$ and fit better for $|\Delta_{a,c1,c2}|/\Omega_{a,c1,c2} = 100$ in the case of two-photon near resonances $\Delta_p \simeq -\Delta_a$ and $\Delta_{c1} \simeq -\Delta_{c2}$.

ORCID iDs

Hui-Min Zhao https://orcid.org/0000-0001-5296-6569
Xiao-Jun Zhang https://orcid.org/0000-0001-8044-897X

References

[1] Liu L F, Zhang Y, Zhang S C, Qian J, Gong S Q and Niu Y P 2022 Magnetic-free unidirectional polarization rotation and free-space optical isolators and circulators *Appl. Phys. Lett.* **121** 261102
[2] Xia K, Nori F and Xiao M 2018 Cavity-free optical isolators and circulators using a chiral cross-Kerr nonlinearity *Phys. Rev. Lett.* **121** 203602
[3] Xia K, Lu G, Lin G, Cheng Y, Niu Y, Gong S and Twamley J 2014 Reversible nonmagnetic single-photon isolation using unbalanced quantum coupling *Phys. Rev.* A **90** 043802
[4] Jalas D *et al* 2013 What is - and what is not - an optical isolator *Nat. Photon.* **7** 579
[5] Bi L, Hu J, Jiang P, Kim D H, Dionne G F, Kimerling L C and Ross C A 2011 On-chip optical isolation in monolithically integrated non-reciprocal optical resonators *Nat. Photon.* **5** 758

[6] Khanikaev A B, Mousavi S H, Shvets G and Kivshar Y S 2010 One-way extraordinary optical transmission and nonreciprocal spoof plasmons *Phys. Rev. Lett.* **105** 126804
[7] Caloz C, Alù A, Tretyakov S, Sounas D, Achouri K and Deck-Léger Z L 2018 Electromagnetic nonreciprocity *Phys. Rev. Appl.* **10** 047001
[8] Bino L D, Silver J M, Woodley M T M, Stebbings S L, Zhao X and Del'Haye P 2018 Microresonator isolators and circulators based on the intrinsic nonreciprocity of the Kerr effect *Optica* **5** 279
[9] Khanikaev A B and Alù A 2015 Nonlinear dynamic reciprocity *Nat. Photon.* **9** 359
[10] Sounas D L, Soric J and Alù A 2018 Broadband passive isolators based on coupled nonlinear resonances *Natl Electron. Rev.* **1** 113
[11] Peng B, Özdemir S K, Lei F, Monifi F, Gianfreda M, Long G L, Fan S, Nori F, Bender C M and Yang L 2014 Parity-time-symmetric whispering-gallery microcavities *Nat. Phys.* **10** 394
[12] Fan L, Wang J, Varghese L T, Shen H, Niu B, Xuan Y, Weiner A M and Qi M 2012 An all-silicon passive optical diode *Science* **335** 447
[13] Chang L, Jiang X, Hua S, Yang C, Wen J, Jiang L, Wang G, Li G and Xiao M 2014 Parity-time symmetry and variable optical isolation in active-passive-coupled microresonators *Nat. Photon.* **8** 524
[14] Bender N, Factor S, Bodyfelt J D, Ramezani H, Christodoulides D N, Ellis F M and Kottos T 2013 Observation of asymmetric transport in structures with active nonlinearities *Phys. Rev. Lett.* **110** 234101
[15] Muñoz de las Heras A and Carusotto I 2022 Optical isolators based on nonreciprocal four-wave mixing *Phys. Rev.* A **106** 063523
[16] Han M, He Y, Li Q, Song X, Wang Y, Yang A, Zeng Q and Peng Y 2023 Efficient optical isolator via dual-Raman process with chiral nonlinearity *Results Phys.* **46** 106288
[17] Graf A, Rogers S D, Staffa J, Javid U A, Griffith D H and Lin Q 2022 Nonreciprocity in photon pair correlations of classically reciprocal systems *Phys. Rev. Lett.* **128** 213605
[18] Sounas D L and Alù A 2017 Non-reciprocal photonics based on time modulation *Nat. Photon.* **11** 774
[19] Yu Z and Fan S 2009 Complete optical isolation created by indirect interband photonic transitions *Nat. Photon.* **3** 91
[20] Sounas D L and Alù A 2014 Angular-momentum-biased nanorings to realize magnetic-free integrated optical isolation *ACS Photonics* **1** 198
[21] Estep N A, Sounas D L, Soric J and Alù A 2014 Magneticfree non-reciprocity and isolation based on parametrically modulated coupled-resonator loops *Nat. Phys.* **10** 923
[22] Kang M S, Butsch A and Russell P S J 2011 Reconfigurable light-driven opto-acoustic isolators in photonic crystal fibre *Nat. Photon.* **5** 549
[23] Shen Z, Zhang Y L, Chen Y, Zou C L, Xiao Y F, Zou X B, Sun F W, Guo G C and Dong C H 2016 Experimental realization of optomechanically induced non-reciprocity *Nat. Photon.* **10** 657
[24] Xu H, Jiang L, Clerk A A and Harris J G E 2019 Nonreciprocal control and cooling of phonon modes in an optomechanical system *Nature* **568** 65
[25] Ruesink F, Mathew J P, Miri M A, Alù A and Verhagen E 2018 Optical circulation in a multimode optomechanical resonator *Nat. Commun.* **9** 1798
[26] Ruesink F, Miri M A, Alù A and Verhagen E 2016 Nonreciprocity and magnetic-free isolation based on optomechanical interactions *Nat. Commun.* **7** 13662
[27] Shen Z, Zhang Y L, Chen Y, Sun F W, Zou X B, Guo G C, Zou C L and Dong C H 2018 Reconfigurable optomechanical circulator and directional amplifier *Nat. Commun.* **9** 1797
[28] Fang K, Luo J, Metelmann A, Matheny M H, Marquardt F, Clerk A A and Painter O 2017 Generalized nonreciprocity in an optomechanical circuit via synthetic magnetism and reservoir engineering *Nat. Phys.* **13** 465
[29] Horsley S A R, Wu J H, Artoni M and La Rocca G C 2013 Optical nonreciprocity of cold atom Bragg mirrors in motion *Phys. Rev. Lett.* **110** 223602
[30] Yang L, Zhang Y, Yan Y B, Sheng Y, Cui C L and Wu J H 2015 Dynamically induced two-color nonreciprocity in a tripod system of a moving atomic lattice *Phys. Rev.* A **92** 053859
[31] Wang D W, Zhou H T, Guo M J, Zhang J X, Evers J and Zhu S Y 2013 Optical diode made from a moving photonic crystal *Phys. Rev. Lett.* **110** 093901
[32] Tang Y and Cohen A E 2010 Optical chirality and its interaction with matter *Phys. Rev. Lett.* **104** 163901
[33] Li T, Miranowicz A, Hu X, Xia K and Nori F 2018 Quantum memory and gates using a Λ-type quantum emitter coupled to a chiral waveguide *Phys. Rev.* A **97** 062318
[34] Lodahl P, Mahmoodian S, Stobbe S, Rauschenbeutel A, Schneeweiss P, Volz J, Pichler H and Zoller P 2017 Chiral quantum optics *Nature* **541** 473
[35] Sayrin C, Junge C, Mitsch R, Albrecht B, O'Shea D, Schneeweiss P, Volz J and Rauschenbeutel A 2015 Nanophotonic optical isolator controlled by the internal state of cold atoms *Phys. Rev.* X **5** 041036
[36] Scheucher M, Hilico A, Will E, Volz J and Rauschenbeutel A 2016 Quantum optical circulator controlled by a single chirally coupled atom *Science* **354** 1577
[37] Zhang S, Hu Y, Lin G, Niu Y, Xia K, Gong J and Gong S 2018 Thermal-motion-induced non-reciprocal quantum optical system *Nat. Photon.* **12** 744
[38] Hu Y Q, Zhang S C and Qi Y H 2019 Multiwavelength magnetic-free optical isolator by optical pumping in warm atoms *Phys. Rev. Appl.* **12** 054004
[39] Zhang S, Lin G, Hu Y, Qi Y, Niu Y and Gong S 2020 Cavity-free circulator with low insertion loss using hot atoms *Phys. Rev. Appl.* **14** 024032
[40] Li E Z *et al* 2020 Experimental demonstration of cavity-free optical isolators and optical circulators *Phys. Rev. Res.* **2** 033517
[41] Liang C, Liu B, Xu A N, Wen X, Lu C, Xia K, Tey M K, Liu Y C and Li Y 2020 Collision-induced broadband optical nonreciprocity *Phys. Rev. Lett.* **125** 123901
[42] Zhang S, Zhan Y, Gong S and Niu Y 2023 Noiseless single-photon isolator at room temperature *Commun. Phys.* **6** 33
[43] Li C, Yu Q, Zhang Y, Xiao M and Zhang Z 2023 Optical isolation with optical parametric amplification in an atomic system *Laser Photon. Rev.* **17** 2200267
[44] Song F, Wang Z P, Li E Z, Yu B L and Huang Z X 2022 Nonreciprocity with structured light using optical pumping in hot atoms *Phys. Rev. Appl.* **18** 024027
[45] Dong M X *et al* 2021 All-optical reversible single-photon isolation at room temperature *Sci. Adv.* **7** eabe8924
[46] Lin G W, Zhang S C, Hu Y Q, Niu Y P, Gong J B and Gong S Q 2019 Nonreciprocal amplification with four-level hot atoms *Phys. Rev. Lett.* **123** 033902

[47] Otterstrom N T, Kittlaus E A, Gertler S, Behunin R O, Lentine A L and Rakich P T 2019 Resonantly enhanced nonreciprocal silicon Brillouin amplifer *Optica* **6** 1117–23
[48] Pucher S, Liedl C, Jin S, Rauschenbeutel A and Schneeweiss P 2022 Atomic spin-controlled non-reciporcal Raman amplification of fiber-guided light *Nat. Photon.* **16** 380–3
[49] Liao K Y, Tu H T, Yang S Z, Chen C J, Liu X H, Liang J, Zhang X D, Yan H and Zhu S L 2020 Microwave electrometry via electromagnetically induced absorption in cold Rydberg atoms *Phys. Rev.* A **101** 053432
[50] Yan D, Gao J W, Bao Q Q, Yang H, Wang H and Wu J H 2011 Electromagnetically induced transparency in a five-level Λ system dominated by two-photon resonant transitions *Phys. Rev.* A **83** 033830
[51] Richardson D J, Fini J M and Nelson L E 2013 Space-division multiplexing in optical fibres *Nat. Photon.* **7** 354
[52] Pasquazi A *et al* 2018 Micro-combs: a novel generation of optical sources *Phys. Rep.* **729** 1–81
[53] Doi Y, Yoshimatsu T, Nakanishi Y, Tsunashima S, Nada M, Kamei S, Sano K and Ishii Y 2020 Receiver integration with arrayed waveguide gratings toward multi-wavelength data-centric communications and computing *Appl. Sci.* **10** 8205
[54] Kittlaus E A, Otterstrom N T, Kharel P, Gertler S and Rakich P T 2018 Non-reciprocal interband Brillouin modulation *Nat. Photon.* **12** 613
[55] Yan W B, Ni W Y, Zhang J, Zhang F Y and Fan H 2018 Tunable single-photon diode by chiral quantum physics *Phys. Rev.* A **98** 043852
[56] Fan C, Shi F, Wu H and Chen Y 2015 Tunable all-optical plasmonic diode based on Fano resonance in nonlinear waveguide coupled with cavities *Opt. Lett.* **40** 2449
[57] Fan S, Qi Y, Lin G, Niu Y and Gong S 2020 Broadband optical nonreciprocity in an N-type thermal atomic system *Opt. Commun.* **462** 125343
[58] Hu Y D and Zhang G Q 2023 Multichannel nonreciprocal amplifications using cesium vapor *Phys. Rev.* A **107** 053716
[59] Fan S, Qi Y, Niu Y and Gong S 2022 Nonreciprocal transmission of multi-band optical signals in thermal atomic systems *Chin. Opt. Lett.* **20** 012701
[60] Steck D A 2023 (available at: https://steck.us/alkalidata/)
[61] Sibalic N, Pritchard J D, Adams C S and Weatherill K J 2021 An introduction to Rydberg atoms with ARC (available at: https://arc-alkali-rydberg-calculator.readthedocs.io/en/latest/Rydberg_atoms_a_primer_notebook.html)
[62] Scully M O and Zubairy M S 1997 *Quantum Optics* (Cambridge University Press)